NWP SAF

Satellite Application Facility
for Numerical Weather Prediction

Document No. NWPSAF–EC–TR–005

Version 1.0

May 2002

Microwave radiative transfer modeling in clouds and precipitation Part I: Model description

Peter Bauer

European Centre for Medium–Range Weather Forecasts

Microwave radiative transfer modeling in clouds and precipitation

Part I: Model description

Peter Bauer

ECMWF

This documentation was developed within the context of the EUMETSAT satellite Application Facility on Numerical Weather Prediction (NWP SAF), under the Cooperation Agreement dated 25 November 1998, between EUMETSAT and the Met Office, UK, by one or more partners within the NWP SAF. The partners in the NWP SAF are the Met Office, ECMWF, KNMI and Météo France.

Change record			
Version	Date	Author / changed by	Remarks

Contents

Abstract

This report gives an overview of microwave radiative transfer modeling in clouds and precipitation. Two model packages are introduced to be made available to the NWP–SAF which are evaluated in part II. Their range of applicability is only limited by the availability of models for the calculation of water and ice permittivity, sea–surface emissivity, and atmospheric absorption. Current models for these ingredients are taken to be valid for the frequency intervals 1–100 GHz, 1–100 GHz, and 1–1000 GHz, respectively. The solution to the radiative transfer equation, however, is general and applies to all wavelengths at which contributions from solar radiation can be neglected, i.e., for which the radiation source terms are only diffuse scattering and thermal radiation. The model package includes pre–calculated tables containing the optical properties of hydrometeors at all microwave frequencies currently available on spaceborne sensors.

1 Introduction

With the increasing computational efficiency of global model processing systems and with the increasing accuracy of convection and cloud schemes the evaluation of model generated radiances with observations and even the assimilation of observed radiances in clouds and precipitation has become an issue. For these applications accurate and fast models for the simulation of the radiative transfer in scattering media are required. For clear–sky conditions, the fast model environment RTTOV (Eyre 1991) has become widely used in the global modeling community. Recently, this package was extended to also cover non–scattering cloud profiles at infrared and microwave wavelengths (English 1999, Chevallier et al. 2001).

This report gives a rather general introduction to the problem of microwave radiative transfer in scattering atmospheres and also presents two models for an efficient and yet accurate simulation of radiances in scattering atmospheres. The two major elements are the radiative transfer codes themselves and the calculation of the optical properties of hydrometeors for a range of electro–magnetic frequencies, temperatures, and hydrometeor contents per hydrometeor type. In part I, both theory and models are compiled while part II (Moreau et al. 2002) presents the model evaluation. The computer codes for all models are available through the authors or the NWP–SAF. They have been revised and unified to Fortran–90 standard. Test input and output files are also available.

2 Microwave radiative transfer

The radiative transfer equation can be expressed as the differential change of radiance L_ν at frequency ν along path s:

$$dL_\nu = -L_\nu k\, ds \tag{1}$$

In vertical coordinates and including slant paths the path coordinate ds is modified to dz/μ with zenith angle $\theta = cos^{-1}\mu$ and altitude z. $k = k_{abs} + k_{sct}$ denotes the volume extinction

coefficient comprising absorption and scattering by all relevant media in the atmosphere. All optical quantities are frequency dependent thus subscript 'ν' will be omitted hereafter.

With the inclusion of source terms and the transformation to (θ, ϕ)–coordinates on a hemisphere with plane–parallel horizon at level z, (1) translates to:

$$\begin{aligned} \mu \frac{dL(z;\mu,\phi)}{k\,dz} &= L(z;\mu,\phi) - J(z;\mu,\phi) \quad (upward), \\ -\mu \frac{dL(z;-\mu,\phi)}{k\,dz} &= L(z;-\mu,\phi) - J(z;-\mu,\phi) \quad (downward) \end{aligned} \tag{2}$$

ϕ denotes the azimuth angle (the angular dependence may be combined to $\Omega = (\mu, \phi), d\Omega = d\mu d\phi$). The source term, J, covers contributions from scattering (hydrometeors) and emission (oxygen, water vapor, dry air, hydrometeors):

$$J(z;\mu,\phi) = \frac{\omega_o}{4\pi} \int_0^{2\pi} \int_{-1}^{1} L(z;\mu',\phi') P(\mu,\phi;\mu',\phi') d\mu' d\phi' + (1-\omega_o) B[T(z)] \tag{3}$$

$\omega_o = k_{sct}/k$ denotes the single scattering albedo and provides a measure for the fraction of scattered radiation while $(1-\omega_o)$ is the fraction of absorbed radiation. $B[T(z)]$ is the blackbody equivalent radiance according to temperature T at level z. Scattering of radiance is expressed in terms of a normalized scattering phase function:

$$\frac{1}{4\pi} \int_0^{2\pi} \int_{-1}^{1} P(\mu,\phi;\mu',\phi') d\mu' d\phi' = 1 \tag{4}$$

describing the distribution of incident radiance (μ', ϕ') to observation direction (μ, ϕ).

The differential form of the radiative transfer equation can be integrated from the surface $(z = 0)$ to the top of the atmosphere, $z = z^*$:

$$\begin{aligned} L(z^*;\mu,\phi) &= \epsilon_{sfc} B(T_{sfc}) \tau(z^*;\mu,\phi) + \\ &+ \int_0^{z^*} J(z';\mu,\phi) exp[-k(z^*-z')/\mu] k\,dz'/\mu + \\ &+ (1-\epsilon_{sfc}) \tau(z^*;\mu,\phi) \int_{z^*}^{0} J(z';\mu,\phi) exp[-k\,z'/\mu] k\,dz'/\mu \end{aligned} \tag{5}$$

with total atmospheric transmission:

$$\tau(z^*;\mu,\phi) = \int_0^{z^*} exp[-k\,z'/\mu] dz' \tag{6}$$

and surface skin temperature, T_{sfc}, and surface emissivity, ϵ_{sfc}, which is a function of frequency, temperature, roughness, foam coverage, and salinity in case of sea water and a function of frequency, temperature, moisture, soil type, vegetation, and roughness (among others) for land surfaces.

2.1 Scattering

In the microwave part of the electromagnetic spectrum, the dependence of scattered radiation on azimuth angle can be neglected in most cases because the diffuse radiation component is much less anisotropic than that originating from a highly anisotropic source such as solar radiation. In this case, the phase function in (4) becomes:

$$P(\mu,\mu') = \frac{1}{2\pi}\int_0^{2\pi} P(\mu,\phi;\mu',\phi')d\phi' \tag{7}$$

and (2) reduces to:

$$\pm\mu\frac{dL(z,\pm\mu)}{k\,dz} = L(z,\pm\mu) - \frac{\omega_o}{2}\int_{-1}^{1} L(z,\mu')P(\pm\mu,\mu')d\mu' - (1-\omega_o)B[T(z)] \tag{8}$$

A rather accurate approximation to the phase function in (7) is given by the Henyey–Greenstein function which is only applicable in scalar radiative transfer that is without including polarization by scattering:

$$P(\pm\mu,\phi;\mu',\phi') = \frac{1-g^2}{(1+g^2-2g\,cos\Theta)^{3/2}} \tag{9}$$

with scattering angle Θ:

$$cos\Theta = \pm\mu\mu' + (1-\mu^2)^{1/2}(1-\mu'^2)^{1/2}cos(\phi-\phi') \tag{10}$$

g denotes the asymmetry parameter which represents the angle averaged phase function, i.e., $g \in [-1,1]$:

$$g = \frac{1}{2}\int_{-1}^{1} P(cos\Theta)cos\Theta\,dcos\Theta = \overline{cos\Theta} \tag{11}$$

This parameter is $> 0/ < 0$ if more radiation is scattered in forward/backward than backward/forward direction. For Rayleigh scattering $g = 0$.

2.2 Polarization

Another important source of information is polarization because surfaces polarize incoming unpolarized radiation by reflection and particles polarize by scattering. In both cases, a strong dependence of illumination vs. observation geometry exists, and the degree and angular distribution of the polarized radiation is determined by surface reflectivity and roughness, and particle scattering efficiency and shape. Polarization calculations require the expansion of radiances into vertically and horizontally polarized components which are elements of the Stokes vector $\mathbf{L} = (I,Q,U,V)$:

$$\begin{aligned} I &= I_h + I_v \\ Q &= I_h - I_v \\ U &= I\,cos2\alpha\,sin2\beta \\ V &= I\,sin2\beta \end{aligned} \tag{12}$$

The (v,h) are defined by a plane between the incoming and scattered/reflected radiation beams. 'v' represents the vertical component and 'h' the parallel component to this plane. Angle β defines the orientation of the vector $\mathbf{L}$ with respect to the 'h'-direction while α stands for the ellipticity of the polarization. The sign of α describes the sense of rotation, i.e., the sign of the phase (Φ) difference between I_h and I_v. Elliptically polarized radiation represents the most general definition form for polarized radiation with special cases of unpolarized, linearly polarized, and circularly polarized radiation thus $I_h = I_v, \beta = 0$; $I_h = I_v, \Phi_h = \Phi_v$; and $I_h/I_v = 1, \Phi_h = \Phi_v \pm \pi/2$, respectively.

The consequence for the radiative transfer equation (8) is that all radiance terms become (Stokes) vectors, scattering and extinction coefficients become matrices while the scattering phase function also becomes a matrix:

$$\pm\mu\frac{d\mathbf{L}(z,\pm\mu,\phi)}{kdz} = \mathbf{L}(z,\pm\mu,\phi) - \frac{\omega_\mathbf{o}}{2}\int_{-1}^{1}\mathbf{I}(z,\mu',\phi')\mathbf{P}(\pm\mu,\phi;\mu',\phi')d\mu'd\phi' - (1-\omega_\mathbf{o})\mathbf{B}[\mathbf{T}(\mathbf{z})] \quad (13)$$

$\mathbf{L}$ is the Stokes vector representation of the scalar intensity, $\mathbf{B}$ is in fact scalar because blackbody emission is unpolarized [$\mathbf{B} = (B,0,0,0)$], $\mathbf{M}$ denotes the 4 x 4 scattering matrix (Mueller matrix), and $\omega_\mathbf{o}$ has also become a 4 x 4 matrix determining the amount of scattering per component. The latter expansion is only required if scattering by non–spherical particles is included, otherwise ω_o remains a scalar.

Since scattering is always described in the local scattering geometry (as is the polarization), i.e., in reference to the plane determined by the incoming and scattered radiation beams with a particle at the center, a coordinate transformation has to be carried out before and after the scattering event with respect to the $(\mu,\phi;\mu',\phi')$ coordinate system:

$$\mathbf{P}(\mu,\phi;\mu',\phi') = \mathbf{F}(i_2-\pi)\mathbf{Q}(cos\Theta)\mathbf{F}(i_1) \quad (14)$$

$\mathbf{F}$ represents a rotation matrix:

$$\mathbf{F}(i) = \begin{pmatrix} 1 & 0 & 0 & 0 \\ 0 & cos2i & -sin2i & 0 \\ 0 & sin2i & cos2i & 0 \\ 0 & 0 & 0 & 1 \end{pmatrix} \quad (15)$$

The most general form of the scattering matrix $\mathbf{Q}$ is:

$$\mathbf{Q}(cos\Theta) = \begin{pmatrix} \frac{M_2+M_3+M_4+M_1}{2} & \frac{M_2-M_3+M_4-M_1}{2} & S_{23}+S_{41} & -D_{23}-D_{41} \\ \frac{M_2+M_3-M_4-M_1}{2} & \frac{M_2-M_3-M_4+M_1}{2} & S_{23}-S_{41} & -D_{23}+D_{41} \\ S_{24}+S_{31} & S_{24}-S_{31} & S_{21}-S_{34} & -D_{21}+D_{34} \\ D_{24}+D_{31} & D_{24}-D_{31} & D_{21}+D_{34} & S_{21}-S_{34} \end{pmatrix} \quad (16)$$

with amplitude functions M_i, S_{ij}, and D_{ij} to be obtained from Mie–calculations (van de Hulst 1957).

(16) can be reduced to a more simple form for spherical particles:

$$\mathbf{Q}(cos\Theta) = \begin{pmatrix} \frac{M_2+M_1}{2} & \frac{M_2-M_1}{2} & 0 & 0 \\ \frac{M_2-M_1}{2} & \frac{M_2+M_1}{2} & 0 & 0 \\ 0 & 0 & S_{21} & -D_{21} \\ 0 & 0 & D_{21} & S_{21} \end{pmatrix} \tag{17}$$

Other simplifications apply for particles with less general symmetry than spheres.

For low microwave frequencies (<20 GHz) and little precipitation, the scatterers may be treated as dipoles thus the Rayleigh scattering formulae for the azimuthally averaged phase function apply with:

$$P_{11}(\pm\mu,\mu') = \frac{3}{4}\left[2(1-\mu^2)(1-\mu'^2) + \pm\mu^2\mu'^2\right] \tag{18}$$
$$P_{12}(\pm\mu,\mu') = \pm\frac{3}{4}\mu^2,\ P_{21}(\pm\mu,\mu') = \frac{3}{4}\mu'^2,\ P_{22}(\pm\mu,\mu') = \frac{3}{4}$$

2.3 Boundaries

Downwelling radiation from space is commonly approximated by $B(2.7K)$ for all incidence angles. Surfaces can be treated as reflectors which are specular for, e.g., a calm water surface. In that case, the Fresnel equations apply which translate to a reflection matrix:

$$\mathbf{R_{sfc}}(\mu,\mu') = \begin{pmatrix} (|r_v|^2+|r_h|^2)/2 & (|r_v|^2-|r_h|^2)/2 & 0 & 0 \\ (|r_v|^2-|r_h|^2)/2 & (|r_v|^2+|r_h|^2)/2 & 0 & 0 \\ 0 & 0 & Re(r_v r_h*) & -Im(r_v r_h*) \\ 0 & 0 & Im(r_v r_h*) & Re(r_v r_h*) \end{pmatrix} \tag{19}$$

Superscript '*' denotes the conjugate complex. With reflection coefficients for a medium with complex permittivity $\epsilon = \epsilon' - i\,\epsilon''$:

$$\begin{aligned} r_h(\mu) &= \frac{(p-\mu)^2+q^2}{p+\mu)^2+q^2} \\ r_v(\mu) &= \frac{(\epsilon'\mu-p)^2+(\epsilon''\mu-q)^2}{(\epsilon'\mu+p)^2+(\epsilon''\mu+q)^2} \\ p &= \frac{1}{\sqrt{2}}\left\{\left[(\epsilon'-\mu-1)^2+\epsilon''^2\right]^{1/2}+(\epsilon'-\mu-1)^2\right\}^{1/2} \\ q &= \frac{1}{\sqrt{2}}\left\{\left[(\epsilon'-\mu-1)^2+\epsilon''^2\right]^{1/2}-(\epsilon'-\mu-1)^2\right\}^{1/2} \end{aligned} \tag{20}$$

Surface transmissivity is neglected in most cases assuming a penetration depth $d_p = \sqrt{\epsilon'}\lambda/(2\pi\epsilon'')$ which is ≈ 0 so that $\epsilon_{\mathbf{sfc}} = 1 - \mathbf{R_{sfc}}$ becomes a matrix in (5). Most natural surfaces, however, are rough so that –at least theoretically– bistatic reflection coefficients have to be calculated giving the fraction of scattered radiation for any incidence and scattering angle combination. Another approximation to surface reflection is represented by a Lambertian reflector for which the distribution of reflected radiation is isotropic over all angles.

3 Radiative transfer models

3.1 Principles

The major problem for radiative transfer modeling is the solution of (3) with (5) because layer interaction can not be solved analytically in case of scattering. Here, simplifications and numerical approaches are required. So far, the radiative transfer equation was expressed by scalar radiances or Stokes vectors in dependence of e.g. zenith angle. Depending on the application and the required accuracy (in particular when multiple scattering is included), even plane–parallel radiative transfer –which assumes constant medium properties in horizontal directions– requires the integration of scattered radiances from the upper and lower half-space into the observation direction. This already appeared in (3).

The angle dimension is treated in the same way as the elements of the Stokes vector or the Mueller matrix so that the dimension of the vectors/matrices does not change. Then:

$$\begin{aligned} \mathbf{L} &= \begin{pmatrix} \hat{\mathbf{L}}(\mu_1) \\ \dots \\ \hat{\mathbf{L}}(\mu_n) \end{pmatrix} \quad \hat{\mathbf{L}}(\mu) = \begin{pmatrix} I(\mu_i) \\ Q(\mu_i) \\ U(\mu_i) \\ V(\mu_i) \end{pmatrix} \\ \mathbf{P}(\mu,\mu') &= \begin{pmatrix} \mathbf{P}(\mu_1,\mu_1) & \dots & \mathbf{P}(\mu_n,\mu_1) \\ \dots & \dots & \dots \\ \mathbf{P}(\mu_1,\mu_n) & \dots & \mathbf{P}(\mu_n,\mu_n) \end{pmatrix} \end{aligned} \tag{21}$$

This aims already at the numerical integration of incoming and scattered radiances into the observation direction by a simple matrix–vector multiplication. To replace the integration by a summation, the Gaussian quadrature formula provides an accurate means for integration in the interval of [-1,1]:

$$\int_{-1}^{1} f(\mu) d\mu \approx \sum_{i=-m}^{m} a_i \, f(\mu_i) \tag{22}$$

At microwave wavelengths, usually less than 16 discrete angles provide enough accuracy, at infrared/visible wavelengths a higher number is required to resolve the stronger anisotropy of the radiance fields.

As mentioned above, the azimuthal dependence is mostly neglected due to the lesser degree of anisotropy. If included, it involves a separation of angle dependencies for the phase function and intensities:

$$\begin{aligned} P(\mu,\phi;\mu',\phi') &= \sum_{m=0}^{N} \sum_{l=m}^{N} \tilde{\omega}_l P_l^m(\mu) P_l^m(\mu') cos(\phi' - \phi) \\ L(z;\mu,\phi) &= \sum_{m=0}^{N} L^m(z,\mu) cos(\phi' - \phi) \end{aligned} \tag{23}$$

where the P_l^m denote the associated Legendre polynominals and:

$$\begin{aligned} \tilde{\omega}_l^m &= (2-\delta_{0,m})\tilde{\omega}_l \frac{(l-m)!}{(l+m)!}, \quad l=m..N, \quad 0 \le m \le N \\ \delta_{0,m} &= \begin{cases} 1 & \text{m} = 0 \\ 0 & \text{otherwise} \end{cases} \end{aligned} \tag{24}$$

Eqs. (2) and (3) would be formulated for each mode I^m and summed according to (23) after integration in the μ–dimension. However, in our case this costly procedure was avoided through the azimuthal averaging.

The equations for the differential radiative transfer have to be formulated for discrete layers assuming that the optical properties do not change through the layer (e.g. by following the layer structure of the input data). Most of the time, the layer temperature is taken to be the average between the bounding levels; however, for optically thick media this assumption produces uncertainties (see below).

The basic formulation originates from the interaction principle, i.e., the linear superposition of contributions from adjacent layers:

$$\begin{aligned} \mathbf{L_1^-} &= \mathbf{T^-}\mathbf{L_0^-} + \mathbf{R^-}\mathbf{L_1^+} + \mathbf{S^-} \\ \mathbf{L_0^+} &= \mathbf{T^+}\mathbf{L_1^+} + \mathbf{R^+}\mathbf{L_0^-} + \mathbf{S^+} \end{aligned} \tag{25}$$

where '+' and '-' denote the upwelling and downwelling radiances, respectively, and $\mathbf{T}$, $\mathbf{R}$, and $\mathbf{S}$ denote the transmission, reflection, and emission operators. At bottom and top of the atmosphere, $L_0^-(z^*) = B(2.7K)$ and at the surface $\mathbf{T^-} = 0$, $\mathbf{R^-}$ is taken from (19) while $\mathbf{S^+} = \epsilon_{\mathbf{sfc}}[B(T_{sfc},\mu_1),0,0,0;...;B(T_{sfc},\mu_n),0,0,0]$.

3.2 Emission

In case of pure emission all reflection matrices are zero and all transmission matrices only contain the diagonal elements so that (neglecting polarization at this point):

$$\begin{aligned} \mathbf{L_1^-} &= \mathbf{T^-}\mathbf{L_0^-} + \mathbf{S^-} \\ \mathbf{L_0^+} &= \mathbf{T^+}\mathbf{L_1^+} + \mathbf{S^+} \end{aligned} \tag{26}$$

with:

$$\begin{aligned} \mathbf{T^\pm} &= \begin{pmatrix} exp(-k\Delta z/\pm\mu_1) & \dots & 0 \\ 0 & \dots & 0 \\ 0 & \dots & exp(-k\Delta z/\pm\mu_n) \end{pmatrix} \\ \mathbf{S^\pm} &= \begin{pmatrix} [1-exp(-k\Delta z/\pm\mu_1)]\,B(T) \\ \dots \\ [1-exp(-k\Delta z/\pm\mu_n)]\,B(T) \end{pmatrix} \end{aligned} \tag{27}$$

For optically thin layers $1-exp(-k\Delta z/\pm\mu_i) \approx k\Delta z/\pm\mu_i$. This can be further simplified if only one zenith angle is used, so that if only the first two elements of the Stokes vector are needed (e.g. to include polarization introduced by surface reflection) (26) has only two elements. This is the form used in current numerical prediction models. Please note, that for the source terms in (27), it was assumed that temperature is constant within the discrete layers. More accurate is a modification to a linear change of temperature with depth. In case of no scattering this can be directly calculated from (46) while for scattering atmospheres, this has to be explicitly included in the numerical integration of layer properties (for details see following chapters).

3.3 Scattering: Doubling/adding

In case of scattering atmospheres, the reflection and transmission matrices include terms of the scattering phase function. The numerical procedure called 'doubling–adding' treats the multiple scattering in layers and the integration of radiances throughout the atmosphere along the following line (e.g. Plass et al., 1973):

1. Starting point is a layer with constant optical properties in the atmosphere (say the upmost layer). This layer has to be divided into sublayers for which single scattering can be assumed. This is usually the case for optical depths $< 10^{-5}$. For a sublayer initial reflection and transmission matrices are calculated. There are various initializations available which produce less different results in the microwave region than at shorter wavelengths (Wiscombe, 1976a). Here, the single–scattering initialization of Chandrasekhar (1960) was implemented:

$$\begin{aligned} \mathbf{R} &= \frac{\omega_o}{2}\mathbf{M}^{-1}\mathbf{P}^{+-}\mathbf{A}\Delta\delta \\ \mathbf{T} &= \mathbf{E} - \mathbf{M}^{-1}k\Delta z + \frac{\omega_o}{2}\mathbf{M}^{-1}\mathbf{P}^{++}\mathbf{A}k\Delta z \\ \mathbf{M} &= \begin{pmatrix} \mu_1 & \dots & 0 \\ 0 & \dots & 0 \\ 0 & \dots & \mu_n \end{pmatrix}, \quad \mathbf{A} = \begin{pmatrix} a_1 & \dots & 0 \\ 0 & \dots & 0 \\ 0 & \dots & a_n \end{pmatrix} \end{aligned} \tag{28}$$

   where the a_i are the weighting coefficients of the Gauss quadrature as in (22). The notation of $\mathbf{P}^{\pm\pm}$ represents the phase function at discrete angles μ_i where the first sign stands for the direction of the incoming radiance and the second for the scattered radiance. Positive signs refer to the lower half space while negative signs refer to the upper half space. The initial operators are independent of viewing direction so that an exchange of viewing direction has no effect. The source term vectors remain as in (27).

2. If two adjacent layers are added (or doubled in case their optical properties are identical) the exiting radiances at top and bottom are:

$$\begin{aligned} \mathbf{L_2^-} &= \mathbf{T_{12}L_1^-} + \mathbf{R_{21}L_2^+} + \mathbf{S_{12}} \\ \mathbf{L_0^+} &= \mathbf{T_{10}L_1^+} + \mathbf{R_{01}L_0^-} + \mathbf{S_{10}} \end{aligned} \tag{29}$$

and those at the layer interface are:

$$\begin{aligned} \mathbf{L_1^-} &= \mathbf{T_{01}L_0^-} + \mathbf{R_{10}L_1^+} + \mathbf{S_{01}} \\ \mathbf{L_1^+} &= \mathbf{T_{21}L_2^+} + \mathbf{R_{12}L_1^-} + \mathbf{S_{10}} \end{aligned} \tag{30}$$

$\mathbf{L_2^-}$ and $\mathbf{L_0^+}$ can also be formulated using combined layer operators:

$$\begin{aligned} \mathbf{L_2^-} &= \mathbf{T_{02}L_0^-} + \mathbf{R_{20}L_2^+} + \mathbf{S_{02}} \\ \mathbf{L_0^+} &= \mathbf{T_{20}L_2^+} + \mathbf{R_{02}L_0^-} + \mathbf{S_{20}} \end{aligned} \tag{31}$$

By inserting (30) in (29) and rearrangement, the combined operators from (31) can be obtained from:

$$\begin{aligned} \mathbf{R_{20}} &= \mathbf{R_{21}} + \mathbf{T_{12}\Gamma^-R_{10}T_{21}} \\ \mathbf{T_{02}} &= \mathbf{T_{12}\Gamma^-T_{01}} \\ \mathbf{S_{02}} &= \mathbf{S_{12}} + \mathbf{T_{12}\Gamma^-(S_{01}} + \mathbf{R_{10}S_{21}}) \\ \mathbf{\Gamma^-} &= [\mathbf{E} - \mathbf{R_{10}R_{12}}]^{-1} = \sum_{i=0}^{\infty} (\mathbf{R_{10}R_{12}})^i \end{aligned} \tag{32}$$

and

$$\begin{aligned} \mathbf{R_{02}} &= \mathbf{R_{01}} + \mathbf{T_{10}\Gamma^+R_{12}T_{01}} \\ \mathbf{T_{20}} &= \mathbf{T_{10}\Gamma^+T_{21}} \\ \mathbf{S_{20}} &= \mathbf{S_{10}} + \mathbf{T_{10}\Gamma^+(S_{21}} + \mathbf{R_{12}S_{01}}) \\ \mathbf{\Gamma^+} &= [\mathbf{E} - \mathbf{R_{12}R_{10}}]^{-1} = \sum_{i=0}^{\infty} (\mathbf{R_{12}R_{10}})^i \end{aligned} \tag{33}$$

The factors $\mathbf{\Gamma^\pm}$ can be interpreted as a multiple reflection / scattering factor.

3. This is carried out successively until the full layer operators are calculated. The sublayer combined operators are computed for optical depths which double the optical depth of the previous layers (starting with the initial layer with $k\Delta z < 10^{-5}$), thus this procedure is called 'Doubling'. All layers of the atmosphere can be treated in the same fashion. As mentioned above, for optically thick media the assumption of an average temperature throughout the doubling process produces errors. For a temperature that changes linearly with optical depth, the adaptation of $B(T) = B_0 + B_1 z$ with z at each doubling step gives much better results.

4. Layers with different optical properties for which the doubling procedure was carried out previously are then combined using the same formulae thus this step is called 'Adding'.

In case of strong scattering, small deviations from the normalization condition given in (4) may occur which may amplify during the doubling process and violate the flux conservation.

This is due to the increasing complexity of the phase function with increasing g which may be undersample by the chosen number of discrete angles. The flux conservation condition is expressed as:

$$\sum_{i=1}^{m} a_i \left(P_{ij}^{++} + P_{ij}^{+-}\right) = 2, \quad j = 1, m \tag{34}$$

Wiscombe (1976b) compiles several correction methods of which the scheme proposed by Grant is used here:

$$\begin{aligned} P_{c,ij}^{+\pm} &= (1 + \epsilon_j \delta_{ij}) P_{ij}^{+\pm} \\ \epsilon_j &= \frac{2 - b_j}{a_j (P_{jj}^{++} + P_{jj}^{+-})} \\ b_j &= \sum_{i=1}^{m} a_i \left(P_{ij}^{++} + P_{ij}^{+-}\right) \end{aligned} \tag{35}$$

Obviously, the correction increments are only added to the diagonal elements which is where they are small compared to the diagonal elements themselves.

3.4 Scattering: Eddington approximation

The Eddington approximation to radiative transfer represents an example for an approximative method. The approximation lies in the development of the radiance vector and phase function to the first order so that only one angle (i.e. the observation angle) is needed and the anisotropic radiance field is decomposed into an isotropic and anisotropic component, respectively:

$$\begin{aligned} L(z, \mu) &= L_o(z) + \mu\, L_1(z) \\ P(cos\Theta) &= 1 + 3\, g\, cos\Theta \end{aligned} \tag{36}$$

so that the source function translates to:

$$J(z, \mu) = [1 - \omega_o(z)] B[T(z)] + \omega_o(z)[L_o(z) + g(z) \mu L_1(z)] \tag{37}$$

for azimuthally averaged fields. g is again the asymmetry parameter.

If these quantities are inserted into (3), two mixed equations are obtained:

$$\begin{aligned} \frac{dL_o(z)}{dz} &= -k(z)\left[1 - \omega_o(z) g(z)\right] L_1(z) \\ \frac{dL_1(z)}{dz} &= -3k(z)\left[1 - \omega_o(z)\right]\left\{L_o(z) - B[T(z)]\right\} \end{aligned} \tag{38}$$

The second derivative of e.g. L_o provides:

$$\frac{d^2 L_o(z)}{dz^2} = \Lambda^2(z)\left\{L_o(z) - B[T(z)]\right\} \tag{39}$$

$$\Lambda^2(z) = 3k^2(z)\left[1 - \omega_o(z)\right]\left[1 - \omega_o(z) g(z)\right] \tag{40}$$

with the general solution:

$$L_o(z) = D_+ exp(\Lambda z) + D_- exp(-\Lambda z) + B[T_o] + B_1 dz \tag{41}$$

A linear dependence of temperature with optical depth is assumed, i.e. $B(T) = B(T_o) + B_1 \Delta z$ with lapse rate B_1.

The coefficients $D_\pm$ are to be obtained from the boundary conditions, i.e., space background radiation, surface emission and reflection as well as with the requirement of flux continuity at the layer boundaries:

$$\left(L_o - \frac{\partial L_o}{h\partial z}\right)_{z=z^*} = 2.7 \tag{42}$$

$$\left(L_o + \frac{\partial L_o}{h\partial z}\right)_{z=0} = \overline{\epsilon}_{v,h} B(T) + (1 - \overline{\epsilon}_{v,h}) \left(L_o - \frac{\partial L_o}{h\partial z}\right)_{z=0} \tag{43}$$

$$\left(L_o + \frac{\partial L_o}{h\partial z}\right)^j_{z=z_i} = \left(L_o + \frac{\partial L_o}{h\partial z}\right)^{j+1}_{z=z_i}$$

where

$$\overline{\epsilon}_{v,h} = 2 \int_0^1 \epsilon_{v,h}(\mu) \mu d\mu \tag{44}$$

and$h = 1.5\, k(1 - \omega_o g)$ and i denotes the i–th layer interface between j-th and (j+1)–th layer.

The Delta–approximation modifies k, ω_o, and g as a consequence of the approximation of the fractional forward peak of the phase function by a delta–function:

$$g' = \frac{g}{1+g}, \quad \omega'_o = \frac{(1-g)^2 \omega_o}{1 - g^2 \omega_o}, \quad k' = (1 - \omega_o g^2) k \tag{45}$$

which has proven to significantly improve the treatment of radiative transfer in two–stream–type models in strongly scattering media. Another modification can be introduced to adapt this model to three–dimensional problems. In that case the upward and downward directed radiances are calculated along the slant path of satellite observations providing a first order approximation to three–dimensional radiative transfer. For media with significant scattering, however, large contributions to the observation originate from outside this beam, i.e., from a larger volume than represented by a single path, so that the accuracy of this approach has limitations.

Having derived the $D_\pm$ for each layer, the source terms, J, are obtained. For those layers where no scattering occurs, the derivation of J is more exact if also the linear dependence of temperature with optical depth in that layer is included. This dependence is usually neglected (i.e. the layer averaged temperature is used) in clear–sky calculations. However, with increasing optical depth, for example in non–scattering clouds, the effective layer temperature may considerably differ from the layer averaged temperature. Therefore, the following solutions are

obtained for upward and downward directed sources:

$$\int_0^{\Delta z} J(z,\mu)\, exp[-k(z)(\Delta z - z)/\mu]dz/\mu = B[T_o](1-\tau) + B_1[\Delta z + \mu/k(\tau - 1)] \quad (46)$$

$$\int_{\Delta z}^{0} J(z,\mu)\, exp[-k(z)z/\mu]dz/\mu = B[T_o](1-\tau) - B_1[\tau\Delta z + \mu/k(\tau - 1)]$$

with $\tau = exp(-k\Delta z/\mu)$.

4 Optical properties

4.1 Atmosphere

At microwave wavelengths, the main atmospheric absorbers are oxygen (O_2) through rotational line absorption between 50–60 GHz as well as 118 GHz; water vapor (H_2O) through rotational line absorption at 22.235 GHz and 183.31 GHz; continuum absorption by water vapor and dry air. Between 1–200 GHz, stratospheric contributions are less important so that the total atmospheric absorption can be computed from profiles of temperature, pressure, and humidity. Models for the simulation of atmospheric absorption are based on laboratory and field measurements under various environmental conditions and have to cover the line intensity, width, and overlap for line absorption as a function of temperature, pressure, and humidity. There are several databases of these measurements available as well as so-called 'line–by–line' models which include contributions from all known absorption lines at the desired frequency. As an example, the Millimeter Propagation Model (MPM) computes local absorption, k_a (in km^{-1}), in terms of a complex atmospheric refractive index $m_a = m'_a - im''_a$ at frequency ν in GHz:

$$\begin{aligned} m_a &= m_o + m'(\nu) + im''(\nu) \\ k_a &= 0.04197\,\nu\, m''(\nu) \end{aligned} \quad (47)$$

The above mentioned contributions are summed up in the imaginary part, $m''(\nu)$ over all absorption lines (in the case of MPM these are 44 oxygen and 30 water vapor lines).

The largest unknown in this frequency range is the water vapor continuum which is rather a correction of a line absorption model. Since these fits are aimed at high accuracy at frequencies near the absorption lines, there may be larger uncertainties in the window regions where the continuum contribution dominates. Another problem is the compatibility of laboratory and field measurements when synthesized in unified models due to representativity of measurements and technical constraints.

4.2 Surface

For a flat sea surface, the emission and reflection could be calculated from the permittivity of water as in (48) and from the Fresnel equations (19) and (20). Surface roughness in case

of non–zero windspeeds as well as foam generation contribute significantly to the modification of the equations. These are treated in different ways. For large gravity waves, the waves are approximated by probability distributions of facet orientations with respect to the viewing angle. For each facet, the Fresnel equations are applied. The distributions depend on wind speed and direction. Facet contributions are integrated to yield the total emission / reflection. Important to notice is that multiple reflection and shadowing of facets at larger roughnesses may be significant

Two–scale models also account for capillary waves and small gravity waves which are superimposed on the large gravity waves. Both components are treated independently where the latter maybe obtained from perturbation theory. Important is the choice of the cut–off frequency to distinguish between the two states. Foam contributions mainly increase ocean emissivity and are parameterized by their fractional coverage and the permittivity of the foam itself. Salinity plays only a role at frequencies below 5 GHz.

The above introduced radiative transfer models employ the fast emissivity model FASTEM–2 (English and Hewison 1998) for an ocean surface–land surfaces are not yet included. An evaluation of FASTEM–2 can be found in Deblonde (2001). The advantage of FASTEM–2 is that it parameterizes the above effects so that computationally efficient simulations of sea surface emissivity for most windpeeds and atmospheric conditions are possible (for 1–100 GHz). However, FASTEM–2 only generates emissivities for one observation direction and not bistatic reflection coefficients. Therefore the off–diagonal elements in (19) are zero which is slightly inaccurate for the doubling–adding model but insignificant for the Eddington model. FASTEM–2 is available through the NWP–SAF and is part of the RTTOV–7+ package.

4.3 Hydrometeors

4.3.1 Particle permittivity

For conducting materials the complex permittivity, $\epsilon = \epsilon' - i\epsilon''$, determines the effect of an external dielectric field on the internal distribution of charges (over time). It is connected to the complex refractive index of that material, $m = m' - im''$, through $m^2 = \epsilon$ thus $\epsilon' = m'^2 - m''^2$, $\epsilon'' = 2m'm''$. Away from the relaxation frequency and for a medium in which friction effects dominate its polarizability the Debye-equations apply:

$$\epsilon' = \epsilon_\infty + \frac{\epsilon_s - \epsilon_\infty}{1 + \omega^2\tau_e^2}, \quad \epsilon'' = \frac{(\epsilon_s - \epsilon_\infty)\omega\tau_e}{1 + \omega^2\tau_e^2} + \frac{\sigma}{\omega\epsilon_o} \tag{48}$$

with $\omega = 2\pi\nu$ and frequency ν, and where τ_e denotes the effective relaxation time, ϵ_s the static permittivity ($\nu \to 0$), ϵ_∞ the high frequency permittivity ($\nu \to \infty$), ϵ_o the permittivity in vacuum and σ the ionic conductivity, respectively. The main effect of ϵ' is the dispersion of the phase delay induced on an electromagnetic wave passing through a medium, while ϵ'' represents the loss of energy.

The available models for the permittivities of water and ice present parameterizations of the above equations with respect to the dependence of their ingredients on temperature and

frequency. Another influence is the effect of soluble materials such as salt as expressed by the second term in (48) for ϵ'' which is only important at frequencies below 5 GHz.

For temperatures above 270 K, most liquid water permittivity models give very similar results. Beyond, their performance depends on how the sparse laboratory measurements were fitted thus how stable the extrapolation is (see difference between permittivity models in Figures 1–3). Among the currently used models, the liquid water model of Liebe et al. (1989) and the ice model of Hufford (1991) were chosen for all permittivity calculations (see model compilation in Mätzler (2001)).

4.3.2 Clouds

The parameterization of the microwave properties of water and ice clouds is based upon two major assumptions: (1) maximum particle size is well below the wavelength thus the Rayleigh approximation to particle scattering and absorption applies and the shape of the size distribution has negligible effects on the derived properties; (2) scattering is negligible thus clouds are treated as pure emitters and transmission, τ, depends only on cloud absorption, thus $\tau = exp(-k_{abs}\Delta z\, cos^{-1}\theta)$ with absorption coefficient k_{abs}, layer depth Δz, and zenith angle θ.

For a monodisperse particle distribution, the liquid water content, w, is calculated from:

$$w = \rho_w \frac{4}{3}\pi \int_o^\infty r'^3 n(r')dr' = \rho_w \frac{4}{3}\pi r^3 N \tag{49}$$

where ρ_w denotes water density, r particle radius, and N total particle number obtained from particle number density, $n(r)$:

$$N = \int_0^\infty n(r')dr' \tag{50}$$

The absorption and scattering coefficients, $k_{abs,sct}$, are obtained from the integration of particle absorption and scattering cross sections, $Q_{abs,sct}$, over the same distribution:

$$k_{abs,sct} = \pi \int_o^\infty Q_{abs,sct}(r')r'^2 n(r')dr' = \pi r^2 N Q_{abs,sct}(r) = \frac{3w}{\rho_w 4r} Q_{abs,sct} \tag{51}$$

If the Rayleigh approximation holds the cross sections are given by (van de Hulst 1957):

$$Q_{abs} = -4xIm\left[\frac{m^2-1}{m^2+2}\right], \quad Q_{sct} = \frac{8}{3}x^4\left|\frac{m^2-1}{m^2+2}\right|^2 \tag{52}$$

which are the first terms of the series expansion used in Mie calculations. $x = 2\pi r/\lambda$ denotes the size parameter with wavelength $\lambda = c/\nu$, speed of light in vacuum c, and frequency ν.

After some manipulation, Eq. (52) for the absorption coefficient is simplified to:

$$k_{abs} = a\left[-Im\left(\frac{m^2-1}{m^2+2}\right)\right] \tag{53}$$

Table 1: Maximum single scattering albedo for water and ice clouds.

Frequency	Max. ω_o Water	Max. ω_o Ice
10.7	0.00000274356	0.000165689
19.4	0.00000901326	0.000544395
22.2	0.0000118011	0.000712723
37.0	0.0000327860	0.00197650
50.3	0.0000606909	0.00364482
89.0	0.000192144	0.0112958
150.0	0.000563904	0.0312341
183.3	0.00122003	0.0457168

where $a = 0.06283813\, m^2\, kg^{-1}\, GHz^{-1}$.

With $m^2 = \epsilon$, Eq. (53) is transferred to:

$$k_{abs} = b \frac{w\, \nu\, \epsilon''}{(\epsilon' + 2)^2 + \epsilon''^2} \tag{54}$$

and $b = 0.18851441\, m^2\, kg^{-1}\, GHz^{-1}$ which holds for both water and ice. Thus (54) requires liquid or ice water contents, frequency and temperature as predictors as well as one of the above models for the complex permittivity of water and ice as a function of frequency and temperature.

Figures 1–3 present results for k_{abs} using several permittivity models (Klein and Swift (1977), Ray (1972) and Liebe et al. (1989) for water and Hufford (1991) and Mishima et al. (1983) for ice) at frequencies of 10.7 GHz, 50.3 GHz, and 150.0 GHz. Black lines indicate full Mie calculations using modified Gamma–distributions adjusted to water contents. The red lines represent the corresponding calculations from (54).

Most importantly, the assumptions made on Rayleigh approximation and size distribution effects hold very well because no significant difference is observed between the curves at all frequencies. Secondly, scattering coefficients are too low (see single scattering albedos, ω_o, in Table 1) to justify a treament of water clouds as grey bodies rather than black bodies (emissivity larger than 0.9988). However, ice clouds may cause problems at higher frequencies with emissivities decreasing to 0.95. The small difference between Mie– and Rayleigh calculations for ice stem from the temperature dependent real part of the complex permittivity which affects mainly the scattering contribution. Here, the assumption of $k_{ext} = k_{abs}$ is slightly inaccurate.

For frozen particles a model for the treatment of air–ice mixtures has to be implemented since for particles with densities below $0.917 g\, cm^{-3}$ air is trapped inside the particle. Depending on the distribution and shape of the air inclusions the permittivity of the mixture changes. In our models, a rather general approach was chosen that is randomly distributed inclusions with elliptical shapes (Bohren and Battan 1982). Three–component mixtures, i.e. melting particles are not considered here. Depending on the application melting particles may be included in future model versions (e.g. Bauer 2001).

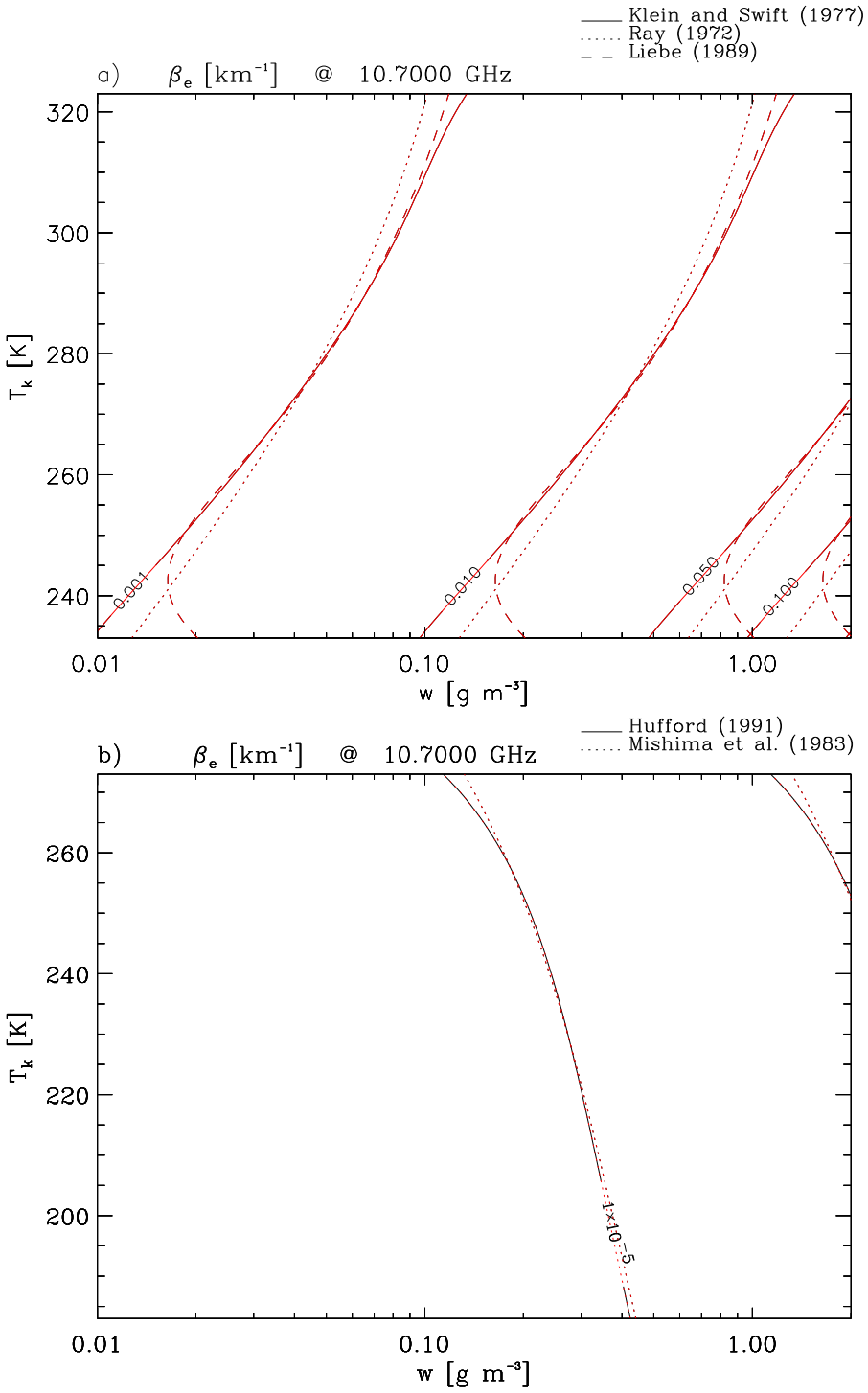

Figure 1: Extinction coefficient from Mie calculations and modified Gamma distributions (black lines) vs. using the Rayleigh approximation and monodisperse distributions (red lines) for water (a) and ice (b) clouds at 10.7 GHz.

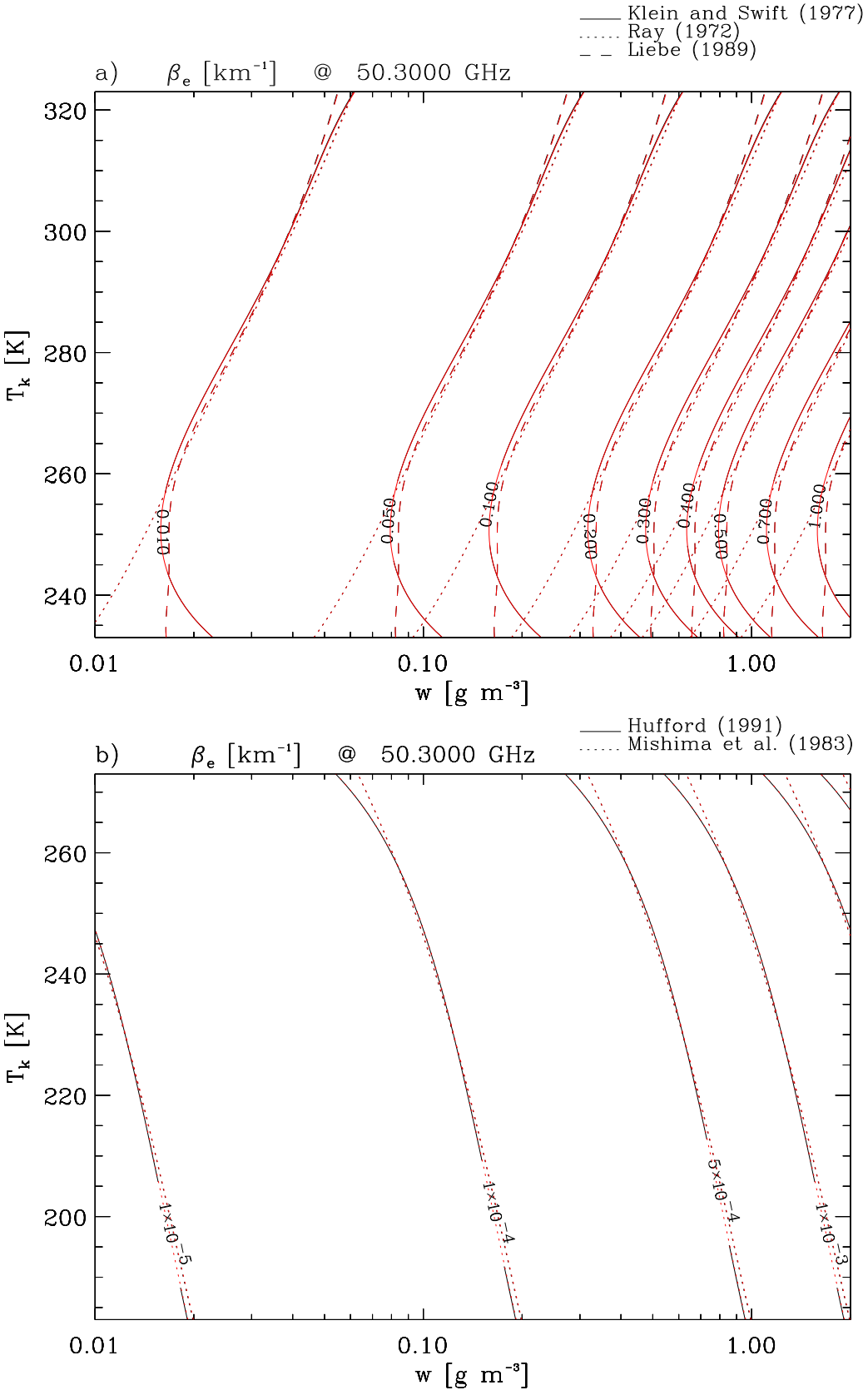

Figure 2: See Figure 1 at 50.3 GHz.

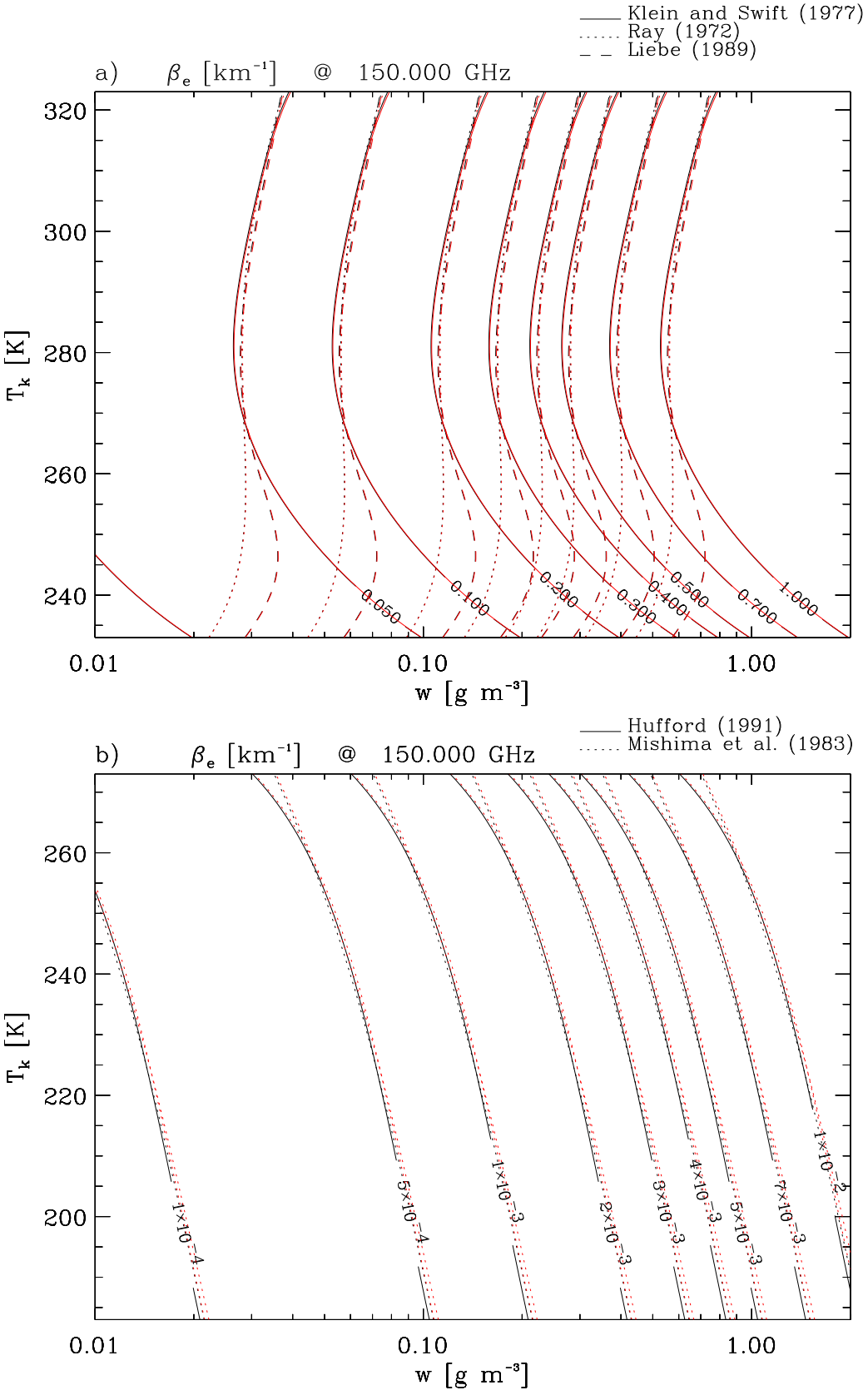

Figure 3: See Figure 1 at 150.0 GHz.

4.3.3 Precipitation

In contrast to non–precipitating cloud particles, liquid and frozen precipitation can not be assumed to have a monodisperse size distribution at the considered frequencies. Size spectra of all precipitating particles are usually calculated from hydrometeor water/ice contents by exponential formulae:

$$N_x(D_x) = N_{o,x} exp(-\Lambda_x D_x) \tag{55}$$

with diameters D_x. To a first order, the intercepts $N_{o,x}$ are set to constant values, e.g., 0.08 cm^{-4} for rain and to 0.04 cm^{-4} for snow or graupel. The index 'x' refers to a specific hydrometeor type. The slope, Λ_x, is then only a function of water/ice content, w_x, and particle density, ρ_x, (both in $g\,m^{-3}$):

$$\Lambda_x = \left(\frac{\pi \rho_x N_{o,x}}{w_x} \right)^{1/4} \tag{56}$$

Equation (56) stems from the solution of the integral over size distribution for the calculation of liquid water contents. The solution is found assuming diameter limits of zero and infinity.

Precipitation rate, R_x, and liquid/ice water content, w_x, are defined as:

$$\begin{aligned} R_x &= \frac{\pi \rho_x}{6} \int_0^\infty N(D_x) V(D_x) D_x^3 dD_x \\ w_x &= \frac{\pi \rho_x}{6} \int_0^\infty N(D_x) D_x^3 dD_x \end{aligned} \tag{57}$$

With an assumption on $V(D_x)$ and $N(D_x)$ direct conversion formulae may be calculated of the form $R_x = e\, w_x^f$.

4.4 Mie–tables

For our purpose, tables of hydrometeor optical properties are calculated for the relevant frequencies, environmental temperatures, and hydrometeor contents. In the case of the doubling–adding model, explicit phase functions are required unless parameterized phase functions are preferred. For the sake of computational efficiency, only the Henyey–Greenstein phase function was implemented so that only extinction coefficient, single scattering albedo, and asymmetry parameter are to be included in the tables. These have to be integrated over the size spectrum for each hydrometeor type:

$$k_{ext}, \omega_o, g, k_{bsct}|_x = \frac{\pi}{4} \int_0^\infty \left[Q_{ext}, \frac{Q_{sct}}{Q_{ext}}, \frac{\overline{cos\theta}}{Q_{sct}}, Q_{bsct} \right] (D_x) N(D_x) D_x^2 dD_x \tag{58}$$

with backscattering, scattering and extinction cross sections Q_{bsct}, Q_{sct} and Q_{ext}, average scattering angle $\overline{cos\theta}$ at frequency ν and temperature T.

Table 2: Microwave frequencies included in Mie–tables.

No.	Frequency [GHz]	Radiometer (channel)
1	1.4	SMOS
2	6.9	AMSR (1–2)
3	10.65	TMI (1–2), AMSR (3–4)
4	18.7	AMSR (3–4)
5	19.35	SSM/I (1–2), TMI (3–4), SSMIS (12–13)
6	21.3	TMI (5)
7	22.235	SSM/I (3), SSMIS (14)
8	23.8	AMSU–A (1), AMSR (5–6)
9	31.4	AMSU–A (2)
10	36.5	AMSR (7–8)
11	37.0	SSM/I (4–5), TMI (6–7), SSMIS (15–16)
12	50.3	AMSU–A (3), SSMIS (1)
13	52.8	AMSU–A (4), SSMIS (2)
14	53.7	AMSU–A (5), SSMIS (3)
15	54.4	AMSU–A (6–7), SSMIS (4)
16	55.5	AMSU–A (8), SSMIS (5)
17	85.5	SSM/I (6–7), TMI (8–9)
18	89.0	AMSU–A (15), AMSU–B (1), AMSR (9–10), MHS (1)
19	91.7	SSMIS (17–18)
20	150.0	AMSU–B (1)
21	157.0	MHS (2)
22	184.3	AMSU–B (5), SSMIS (11), MHS (3)
23	186.3	AMSU–B (4), SSMIS (10), MHS (4)
24	190.3	AMSU–B (3), SSMIS (9), MHS (5)
25	190.3	AMSU–B (3), SSMIS (9), MHS (5)

The contributions from co–existing hydrometeor types are integrated by:

$$\begin{aligned} k_{ext} &= \sum_j k_{ext,x}, \quad j = r,s,g,h,w,i \\ \omega_o &= \frac{\sum_j \omega_{o,x}\, k_{ext,x}}{\sum_j k_{ext,x}} \\ g &= \frac{\sum_j g_x\, \omega_{o,x}\, k_{ext,x}}{\sum_j \omega_{o,x}\, k_{ext,x}} \\ k_{bsct} &= \frac{\sum_j k_{bsct,x}\, k_{ext,x}}{\sum_j k_{ext,x}} \end{aligned} \tag{59}$$

Indices (r,s,g,h,w,i) refer to rain, snow, graupel, hail, cloud liquid water and cloud ice.

The tables use the following discretization:

- 25 frequencies covered by currently available passive microwave radiometers assuming monochromatic center frequencies, i.e., negligible bandwidths (see Table 2).
- 6 hydrometeor types: rain, snow, graupel, hail, cloud liquid water and cloud ice. For details on assumptions for size distributions and densities refer to Bauer (2001).
- 70 temperature indices: for liquid particles $i = T - 233\,K$ thus $T \in [234, 303\,K]$, for frozen particles $i = T - 203\,K$ thus $T \in [204, 273\,K]$.
- 401 liquid/ice water indices: $j = 10 \cdot dB(w_x)$ or $j = 100 \cdot log_{10}(w_x)$ thus $w_x \in [0.001, 10\,g\,m^{-3}]$.

References

Bauer, P., 2001: Including a melting layer in microwave radiative transfer simulation for clouds. *Atmos. Res.*, **57**, 9–30.

Bohren, C.F. and L.J. Battan, 1982: Radar backscattering of microwaves by spongy ice spheres. *J. Atmos. Sci.*, **39**, 2623–2629.

Chandrasekhar, S., 1960: Radiative transfer. Dover Publications Inc., New York, 303 pp.

Chevallier, F., P. Bauer, G. Kelly, C. Jalob, and T. McNally, 2001: Model clouds over oceans as seen from space: Comparison with HIRS/2 and MSU radiances. *J. Climate*, **14**, 4216–4229.

Deblonde, G., 2001: Evaluation of FASTEM and FASTEM–2. NWP–SAF report, available from NWP–SAF hosted by The Met Office, Bracknell UK, 53 pp.

English, S., and T.J. Hewison, 1998: A fast generic millimetre wave emissivity model. In *Proceedings of the International Society for Optical Engineering (SPIE) on Microwave Remote Sensing of the Atmosphere and Environment*, T. Hayasaka, D.L. Wu, Y.–Q. Jin, J.–S. Jiang (Eds.), **3503**, 22–30.

Eyre, J.R., 1991: A fast radiative transfer model for satellite sounding systems. ECMWF Tech. Memo. No. 176, 28 pp.

Hufford, G.A., 1991: A model for the complex permittivity of ice. *Int. J. Infrared Millimeter Waves*, **12**, 677–681.

Klein, L.A. and C.T. Swift, 1977: An improved model for the dielectric constant of sea water at microwave frequencies. *IEEE Trans. Antennas Propag.*, **25**, 104–111.

Liebe, H.J, T. Manabe, and G.A. Hufford, 1989: Millimeter wave attenuation and delay rates due to fog/cloud conditions. *IEEE Trans. Antennas Propag.*, **37**, 1617–1623.

Mätzler (Ed.), 2000: Radiative transfer models for microwave radiometry. Report to COST action 712, available from European Commission, DG–R, rue de la Loi/Wetstraat 200 (SDME 1/53), B–1049 Brussels, 173 pp.

Moreau, E., P. Bauer, and F. Chevallier, 2002: Microwave radiative transfer modeling in clouds

and precipitation. Part II: Model evaluation. NWP–SAF report No. 5, available from NWP–SAF hosted by The Met Office, Bracknell UK, 21 pp.

Mishima, O., D.D. Klug, and E. Whalley, 1983: The far-infrared spectrum of ice Ih in the range of 8-25 cm. Part I: Sound waves and difference bands with application to Saturn's rings. *J. Chem. Phys.*, **78**, 6399–6404.

Plass, G.N., G.W. Kattawar, and F.E. Catchings, 1973: Matrix operator theory. 1: Rayleigh scattering. *Appl. Optics*, **12**, 314–329.

Ray, P., 1972: Broadband complex refractive indices of ice and water. *Appl. Opt.*, **11**, 1836–1844.

van de Hulst, H.C., 1957: Light scattering by small particles. John Wiley and Sons, N.Y., 470 pp.

Wiscombe, W.J., 1976a: Extension of the doubling method to inhomogeneous sources. *J. Quant. Spectrosc. Radiat. Transfer*, **16**, 477–489.

Wiscombe, W.J., 1976b: On initialization, error and flux conservation in the doubling method. *J. Quant. Spectrosc. Radiat. Transfer*,**16**, 637–658.

A Program structure

The radiative transfer program package contains the following routines and files:

- A routine for testing the models:

  `test_eddington.f90`

- a module containing global parameters:

  `mod_rt.f90`

- the two models:

  `matrix_operator.f90 eddington.f90`

- math routines for matrix inversion and for solving a system of linear equations:

  `minv.f90 math.f`

- test input datasets (see chapter 'Comparison with other models' in part II):

  `mt_cohmex op_cohmex`

- corresponding output:

  `matrix_operator.output eddington.output`

The package for the calculation of Mie–tables contains:

- The main program and subroutine library:

  `create_tables_spectra.f90 create_tables_lib.f90`

- a module containing global parameters:

  `mod_mie.f90`

The sequence of subroutine calls is:

```
program test_matrix_operator

   loop over profiles
      loop over frequencies

         CALL doubling_adding
            CALL set_stuff                    | set matrices M, A (28)
            CALL set_prof                     | calculate all layer quantities

            CALL henyey_greenstein            | phase function (9), averaging (7)
            CALL renormalize                  | ensure flux conservation (35)

            CALL doubling                     | single layer operators
               loop over number of doublings
                  CALL mrf                    | sublayer-sublayer multiple scattering term (32, 33)
                  CALL minv                   | matrix inversion (32, 33)
                  CALL add_t                  | sublayer-sublayer transmission (32, 33)
                  CALL add_r                  | sublayer-sublayer reflectivity (32, 33)
                  CALL add_s                  | sublayer-sublayer source term (32, 33)

            CALL adding                       | combine layers
               loop over layers
                  CALL mrf                    | layer-layer multiple scattering term (32, 33)
                  CALL minv                   | matrix inversion (32, 33)
                  CALL add_t                  | layer-layer transmission (32, 33)
                  CALL add_r                  | layer-layer reflectivity (32, 33)
                  CALL add_s                  | layer-layer source term (32, 33)

            CALL mrf                          | surface-atmosphere multiple scattering term (32, 33)
            CALL add_t                        | surface-atmosphere transmission (32, 33)
            CALL add_r                        | surface-atmosphere reflectivity (32, 33)
            CALL add_s                        | surface-atmosphere source term (32, 33)

      end loop
   end loop
end program test_matrix_operator
```

```
program test_eddington

   loop over profiles
      loop over frequencies
         loop over angles

              CALL eddington                  | vertical polarization
                 CALL set_prof                | calculate all layer quantities
                 CALL boundary_conditions     | get D+ and D- in (41)
                    CALL lulu                 | solve system of linear equations

                 CALL integrate_source        | integrate J (37) over layer depths

              CALL eddington                  | horizontal polarization
       ... (as above)

         end loop
      end loop
   end loop
end program test_eddington
```

```
program create_tables_spectra

   loop over frequencies
      loop over hydrometeor types
         loop over temperatures

            CALL perm_water                  | parameterization of (47) for water
            CALL perm_ice                    | parameterization of (47) for ice
            CALL mg_ellips                   | dielectric mixing for ice

    loop over liquid/ice water contents
       loop over cloud droplet sizes

  CALL mie_sphere             | Mie single scattering properties
  CALL mod_gamma_dsd          | Modified gamma size distribution

               end loop

       CALL gamma_dsd                 | Gamma size distribution [(54) for exponential]

       loop over precipitating particle sizes

  CALL mie_sphere             | Mie single scattering properties

            end loop
         end loop
      end loop
   end loop
```